

Asymptotic Anytime-Valid Inference for U-statistics

Leheng Cai^{*‡}, Qirui Hu^{†‡§} and Weijia Li^{*‡}

Abstract

We study asymptotic anytime-valid confidence sequences for degree-two U-statistics under continuous monitoring. In the nondegenerate case, Hoeffding’s projection reduces the problem to a time-uniform central limit theory for the partial sums of the first-order projection, while the canonical remainder is shown to be negligible under mild moment assumptions. A leave-one-out jackknife estimator then yields a fully data-driven procedure, leading to confidence sequences with asymptotic coverage guarantee for the parameter of interest. In the degenerate case, we show that the U-statistic is approximated by a centered quadratic Gaussian-chaos rather than by a simple Gaussian, which poses significant challenges for sequential inference. To address this issue, we novelly develop the Spectrally Allocated Gaussian-chaos Excursion (SAGE) boundary, and then provide plug-in implementations based on truncated spectrum estimation with consistency guarantees. The resulting widths can attain the expected time-uniform optimal rates: $\sqrt{\log \log n/n}$ in the nondegenerate regime and $\log \log n/n$ in the degenerate regime. Several widely used U-statistics are discussed within the proposed framework, and numerical experiments further support the validity of the derived theory.

1 Introduction

U-statistics are a typical device for estimating distributional functionals that can be written as expectations of symmetric kernels. Since Hoeffding’s decomposition, they have served as a unifying language for rank statistics, variance and covariance estimation, measures of dispersion and association, and two-sample or independence testing [19, 36, 25, 24, 27, 21, 26]. Their appeal is not only unbiasedness: the same projection calculus gives classical limit theory and separates the regular first-order component from genuinely second-order behavior. In the nondegenerate regime, the first Hoeffding projection reduces the leading term to an average of i.i.d. influence functions, while in the canonical degenerate regime, the projection vanishes and the statistic is instead a quadratic form or Gaussian chaos, with limit laws depending on the spectrum of the associated integral operator [17, 9, 7, 1, 8, 14, 13].

^{*}Tsinghua University

[†]Shanghai University of Finance and Economics

[‡]The authors are listed in alphabetical order with equal contribution

[§]Corresponding author: huqirui@mail.shufe.edu.cn

This dichotomy is especially relevant in modern machine learning and nonparametric distributional inference. Kernel maximum mean discrepancy (MMD), Hilbert–Schmidt independence criteria, energy distances, and distance covariance are all naturally expressed through U- or V-statistics; under the null hypothesis of equality or independence, their first-order projections typically vanish, producing the weighted chi-square or Gaussian-chaos null limits [16, 2, 39, 38, 35]. Thus, the degenerate case is not a pathological corner case. It is the operating regime of many distributional tests. At the same time, it is the regime in which calibration is most delicate, because the boundary depends on spectral quantities that are usually unknown and must be estimated from the same data stream [23, 34].

Anytime-valid inference asks for uncertainty statements that remain valid under continuous monitoring and optional stopping. For sample means and related estimating equations, this goal is now well understood through nonnegative martingales, test supermartingales, mixture boundaries, and betting constructions [40, 6, 32, 33, 20, 42, 31]. These methods give finite-sample confidence sequences (CSs) when enough structure is available, for example boundedness, sub-exponential tails, or an exact martingale estimating equation. A complementary line of work develops asymptotic confidence sequences (AsympCSs) by replacing fixed-time central limit approximations with time-uniform strong approximations, thereby recovering CLT-like versatility in sequential settings [41, 15].

For U-statistics, however, the usual mean-based sequential tools do not transfer directly. Adding a new observation changes all pairs involving that observation, so the statistic is not a sum of independent increments. Even in the nondegenerate case, the reduction to a sample mean is only asymptotic and must be uniform over all monitoring times; a fixed-time CLT does not control the event of ever crossing a boundary. One must prove that the canonical Hoeffding remainder is almost surely negligible relative to the iterated-logarithm order, and any plug-in estimation does not disturb time-uniform coverage. Notably, the degenerate case is much harder: there is no Brownian first-order limit, the correct width is of order $\log \log n/n$ rather than $\sqrt{\log \log n/n}$, and a boundary must control a countable quadratic Gaussian chaos with unknown signed eigenvalues.

There is a substantial sequential literature around U-statistics, but it addresses different inferential targets. Classical work studied fixed-width or two-stage sequential confidence procedures and stopping times based on U-statistics [37, 28, 29, 30]. More recent work has used U-statistic processes for retrospective or online change-point detection, including robust Wilcoxon-type monitoring and distributional monitoring based on degenerate U-statistics [10, 11, 22, 3]. These contributions are closely related in motivation, but their calibration is designed for testing change-points or for prescribed stopping rules. They do not provide a general AsympCS for a fixed degree-two U-functional, and they do not give a unified treatment of the nondegenerate and canonical degenerate regimes with data-driven spectral calibration.

This paper fills that gap by developing asymptotic anytime-valid inference for degree-two U-statistics under continuous monitoring. Our central idea is to separate the construction into two components: a probabilistic approximation that holds uniformly over time, and a statistical calibration step that estimates the nuisance quantities appearing in the limiting boundary. This separation yields a modular framework and clarifies precisely where moment conditions, degeneracy, and spectral estimation enter. In the nondegenerate regime, we show that the

relevant limiting object is a Brownian partial-sum process associated with the first Hoeffding projection. Based on an almost sure Gaussian approximation and a strongly consistent jackknife variance estimator (Theorems 1 and 2), we construct AsympCSs; see Theorem 3. These sequences connect naturally to classical time-uniform Gaussian boundaries; in particular, the stitched law-of-the-iterated-logarithm boundary achieves the optimal width $\sqrt{\log \log n/n}$.

In the degenerate regime, the limiting object is instead a centered quadratic Gaussian-chaos process. For this case, we derive a Gaussian-chaos approximation and novelly develop the Spectrally Allocated Gaussian-chaos Excursion (SAGE) boundary; see Theorems 4 and 5, which allocates the significance level budget across spectral coordinates and yields an AsympCS with the canonical $\log \log n/n$ scale, matching the law-of-the-iterated-logarithm behavior of canonical degree-two U-statistics. We then provide data-driven plug-in procedures for the degenerate regime based on truncated empirical spectral estimation. Finally, we illustrate the scope of the framework through common examples, including sample variance, Gini mean difference, spatial Kendall's tau and MMD. To our best knowledge, this paper first addressed the asymptotic anytime-valid inference for U-statistics systematically.

The rest of the paper is organized as follows. Section 2 fixes notations, recalls Hoeffding's decomposition, defines AsympCSs, and states the Gaussian boundaries used in the constructions. Section 3 gives the nondegenerate and degenerate theoretical guarantees. Section 4 collects concrete examples of U-statistics. Section 5 contains simulation designs and numerical results. Section 6 concludes. Detailed proofs and additional numerical results are deferred to the appendix.

2 Preliminaries

Hoeffding decomposition. Let X_1, \dots, X_n be i.i.d. random elements taking values in \mathcal{X} . Consider the second-order U-statistic

$$U_n = \binom{n}{2}^{-1} \sum_{1 \leq i < j \leq n} h(X_i, X_j),$$

where $h : \mathcal{X}^2 \rightarrow \mathbb{R}$ is a symmetric kernel satisfying $\mathbb{E}h^2(X_1, X_2) < \infty$. Let $\theta = \mathbb{E}h(X_1, X_2)$ be the parameter of interest. Define the first-order projection $h_1(x) = \mathbb{E}\{h(x, X_2)\} - \theta$, and the canonical kernel $h_2(x, y) := h(x, y) - \theta - h_1(x) - h_1(y)$. Hoeffding's decomposition gives

$$U_n - \theta = \frac{2}{n} \sum_{i=1}^n h_1(X_i) + R_n, \quad R_n := \binom{n}{2}^{-1} \sum_{1 \leq i < j \leq n} h_2(X_i, X_j). \quad (1)$$

We call the U-statistic nondegenerate if $\text{Var}(h_1(X_1)) > 0$, and degenerate (canonical) if $h_1(X_1) = 0$ almost surely. For degenerate U-statistics, let $\mathcal{K} : L^2(\mathbb{P}) \rightarrow L^2(\mathbb{P})$ be the Hilbert-Schmidt operator $(\mathcal{K}f)(x) = \int \{h(x, y) - \theta\} f(y) d\mathbb{P}(y)$. Then \mathcal{K} is compact and self-adjoint, and admits the spectral expansion in $L^2(\mathbb{P} \times \mathbb{P})$, i.e. for the eigensystems $(\lambda_\ell, \psi_\ell)_{\ell \geq 1}$ of \mathcal{K} ,

$$h(x, y) - \theta = \sum_{\ell \geq 1} \lambda_\ell \psi_\ell(x) \psi_\ell(y). \quad (2)$$

Asymptotic anytime-valid sequential inference. In this paper, we adopt the following framework of asymptotic anytime-valid inference [41].

Definition 1 (AsympCSs). *Let \mathcal{T} be a totally ordered infinite set. The intervals $\left[\widehat{\theta}_t - \ell_t, \widehat{\theta}_t + u_t\right]_{t \in \mathcal{T}}$ with $\ell_t, u_t > 0$ form an $(1 - \alpha)$ -AsympCS for a sequence of real parameters $\{\theta_t\}_{t \in \mathcal{T}}$ if there exists a (typically unknown) non-asymptotic $(1 - \alpha)$ -CS $\left[\widehat{\theta}_t - \ell_t^*, \widehat{\theta}_t + u_t^*\right]_{t \in \mathcal{T}}$ such that the probability $\mathbb{P}\left(\forall t \in \mathcal{T}, \theta_t \in \left[\widehat{\theta}_t - \ell_t^*, \widehat{\theta}_t + u_t^*\right]\right) \geq 1 - \alpha$, and $\ell_t^*/\ell_t \xrightarrow{a.s.} 1$, $u_t^*/u_t \xrightarrow{a.s.} 1$.*

Unlike existing nonasymptotic inference results for means of random variables, which often rely on strong boundedness or moment-generating-function assumptions [42, 20], this asymptotic framework allows us to establish universal closed-form boundaries for both nondegenerate and degenerate U -statistics under mild moment conditions.

On the other hand, a central tool for constructing AsympCSs for the mean of i.i.d. random variables is a time-uniform boundary for Gaussian partial sums [41], of which the formal definition is given below.

Definition 2 (Gaussian boundary). *Fix $\alpha \in (0, 1)$. A map $\gamma_{\alpha, m} : \mathbb{N} \rightarrow (0, \infty)$ is called a $(1 - \alpha)$ Gaussian boundary starting from m if, for i.i.d. standard Gaussian random variables $\{Z_i\}_{i \in \mathbb{N}}$,*

$$\mathbb{P}\left(\forall n \geq m : \left|\frac{1}{n} \sum_{i=1}^n Z_i\right| \leq \gamma_{\alpha, m}(n)\right) \geq 1 - \alpha. \quad (3)$$

The starting point m marks the end of the cold-start phase. Several standard choices of the boundary $\gamma_{\alpha, m}(\cdot)$ are available for non-asymptotic CSs of Gaussian means in the literature. A representative example is the stitched boundary of [20], which achieves the concentration rate $\mathcal{O}\left(\sqrt{\log \log n/n}\right)$:

$$\gamma_{\alpha, m}^{\text{LIL}}(n) = \frac{\eta^{1/4} + \eta^{-1/4}}{\sqrt{2n}} \sqrt{s \log \log \left(\max\left\{\frac{\eta n}{m}, e\right\}\right) + \log \frac{\zeta(s)}{\alpha(\log \eta)^s}}, \quad (4)$$

where $\eta, s > 1$, and $\zeta(\cdot)$ is the Riemann zeta function.

Another classical construction is Robbins' Gaussian mixture boundary [32, 33], which attains the rate $\mathcal{O}\left(\sqrt{\log n/n}\right)$:

$$\gamma_{\alpha, m}^{\text{GM}}(n) = \sqrt{\left[\{g^{-1}(\alpha)\}^2 + \log(n/m)\right]/n}, \quad \text{where } g(a) = 2\{1 - \Phi(a) + a\phi(a)\}. \quad (5)$$

Here, $\Phi(\cdot)$ and $\phi(\cdot)$ denote the CDF and PDF of a standard Gaussian distribution, respectively. These bounds will be used as building blocks for our proposed anytime-valid inference procedure for U -statistics.

3 Main results

Non-degenerate case. We first consider that the kernel is non-degenerate at the first order, i.e., $\sigma^2 := \text{Var}\{h_1(X_1)\} > 0$.

The Hoeffding decomposition in (1) implies that the leading behavior of a nondegenerate second-order U -statistic is governed by an average of i.i.d. first-order projections. By establishing an almost sure Gaussian approximation for the first Hoeffding projection with positive variance and showing that the canonical remainder is asymptotically negligible almost surely, Theorem 1 rigorously shows that the nondegenerate U -statistic can be approximated almost surely by the mean of a sequence of i.i.d. Gaussian random variables.

Theorem 1. *Suppose that $\mathbb{E}|h(X_1, X_2)|^{2+\delta} < \infty$ for some $\delta > 0$, and that the kernel is non-degenerate at the first order, i.e., $\sigma^2 > 0$. On an enriched probability space there exists i.i.d. standard Gaussian random variables Z_1, \dots, Z_n such that*

$$\left| U_n - \theta - \frac{2\sigma}{n} \sum_{i=1}^n Z_i \right| = o_{a.s.}(n^{-1+1/(2+\delta)}).$$

We consider the jackknife-type variance estimator for the unknown variance σ^2 in Theorem 1,

$$\hat{\sigma}_n^2 = \frac{1}{n} \sum_{i=1}^n \left\{ \frac{1}{n-1} \sum_{j \neq i} h(X_i, X_j) \right\}^2 - U_n^2. \quad (6)$$

The following Theorem 2 establishes the strong consistency of $\hat{\sigma}_n^2$.

Theorem 2. *Suppose that $\mathbb{E}|h(X_1, X_2)|^4 < \infty$. The variance estimator $\hat{\sigma}_n^2$ defined in (6) is strongly consistent: $|\hat{\sigma}_n^2 - \sigma^2| = \mathcal{O}_{a.s.}(\sqrt{\log \log n/n})$.*

For classical asymptotic inference for non-degenerate U -statistics, one typically applies the central limit theorem and uses non-asymptotic standard normal quantiles as critical values to construct asymptotic confidence intervals (CIs). Motivated by Theorem 1 and the analogy with classical asymptotic inference, we use Gaussian boundaries to construct AsympCSs. The following Theorem 3 provides the corresponding theoretical justification.

Theorem 3. *Suppose that $\mathbb{E}|h(X_1, X_2)|^4 < \infty$. Then, $[U_n \pm 2\hat{\sigma}_n \gamma_{\alpha, m}(n)]_{n \geq m}$ forms a $(1 - \alpha)$ -AsympCS for θ starting from m . Furthermore,*

$$\liminf_{m \rightarrow \infty} \mathbb{P} \{ \forall n \geq m : \theta \in [U_n \pm 2\hat{\sigma}_n \gamma_{\alpha, m}(n)] \} \geq 1 - \alpha. \quad (7)$$

By plugging in the Gaussian boundaries in (4) or (5), we obtain universal AsympCSs for nondegenerate U -statistics. In particular, the plug-in boundary based on (4) achieves the optimal rate, since the law of the iterated logarithm for nondegenerate U -statistics yields

$$\limsup_{n \rightarrow \infty} \sqrt{n/(2 \log \log n)} |U_n - \theta| = 2\sigma, \quad \text{a.s.}$$

In addition, we note that as long as σ^2 admits a polynomial-rate estimator rather than merely an arbitrary $\mathcal{O}_{a.s.}(1)$ -consistent estimator, the resulting AsympCS enjoys the asymptotic time-uniform coverage guarantee in (7).

Degenerate case. We now consider the canonical case, where $h_1(X_1) = 0$ almost surely. In this regime, the U -statistic is no longer dominated by the first-order projection in the Hoeffding decomposition; instead, it is entirely the second-order degenerate component. Consequently, its asymptotic behavior changes significantly.

The following Theorem 4 shows that the degenerate U -statistic admits an almost sure approximation by a centered quadratic Gaussian chaos process.

Theorem 4. *Assume that $\mathbb{E} \{h(X, X') \log |h(X, X')|\}^2 + \mathbb{E} \{h(X, X) \log |h(X, X)|\}^2 < \infty$ and the kernel is degenerate at the first order, i.e., $\sigma^2 = 0$. On an enriched probability space there exist independent standard Brownian motions $\{W_\ell(\cdot)\}_{\ell \geq 1}$ such that one has*

$$\left| U_n - \theta - n^{-2} \sum_{\ell \geq 1} \lambda_\ell \{W_\ell^2(n) - n\} \right| = \mathcal{O}_{a.s.}(\log \log n/n), \quad (8)$$

where $\{\lambda_\ell\}_{\ell \geq 1}$ are the eigenvalues defined in (2).

Let $(\beta_{\ell,n})_{\ell \geq 1}$ be a nonnegative weight array with $\sum_{\ell \geq 1} \beta_{\ell,n} = 1$, and we write β_ℓ for $\beta_{\ell,n}$ for simplicity. Let $\Lambda = \sum_{\ell \geq 1} \lambda_\ell$, $\Lambda^+ = \sum_{\ell: \lambda_\ell > 0} \lambda_\ell$, $\Lambda_\beta^+ = \sum_{\ell: \lambda_\ell > 0} \lambda_\ell \log(1/\beta_\ell)$ and $\Lambda_{\beta,g}^+ = \sum_{\ell: \lambda_\ell > 0} \lambda_\ell \{g^{-1}(\alpha\beta_\ell)\}^2$, where $g(a) = 2\{1 - \Phi(a) + a\phi(a)\}$. We now introduce the Spectrally Allocated Gaussian-chaos Excursion (SAGE) boundary $\Upsilon_{\alpha,m}(\cdot)$, for controlling quadratic Gaussian-chaos processes. For a fixed significance level $\alpha \in (0, 1)$, we distribute the budget α across the Brownian coordinates by setting $\alpha_\ell = \alpha\beta_\ell$, apply a Gaussian mean boundary to each $W_\ell(\cdot)$, combine the coordinatewise guarantees via a union bound, and aggregate the resulting bounds with the spectral weights λ_ℓ . This yields the following time-uniform upper boundary for the centered quadratic Gaussian-chaos process.

Theorem 5. *Suppose that $\sum_{\ell \geq 1} |\lambda_\ell| < \infty$, $\Lambda_\beta^+ < \infty$ and $\{W_\ell(\cdot)\}_{\ell \geq 1}$ are independent standard Brownian motions. For any $\alpha \in (0, 1)$, $m \geq 1$,*

$$\mathbb{P} \left(\forall n \geq m : n^{-2} \sum_{\ell \geq 1} \lambda_\ell \{W_\ell^2(n) - n\} \leq \Upsilon_{\alpha,m}(n) \right) \geq 1 - \alpha,$$

where $\Upsilon_{\alpha,m}(n)$ can be chosen in either of the following two ways:

$$\Upsilon_{\alpha,m}^{LIL}(n) = \frac{(\eta^{1/4} + \eta^{-1/4})^2}{2n} \left[\left\{ s \log \log \left(\max \left\{ \frac{\eta n}{m}, e \right\} \right) + \log \frac{\zeta(s)}{\alpha (\log \eta)^s} \right\} \Lambda^+ + \Lambda_\beta^+ \right] - \frac{\Lambda}{n}, \quad (9)$$

$$\Upsilon_{\alpha,m}^{GM}(n) = n^{-1} [\Lambda^+ \log(n/m) + \Lambda_{\beta,g}^+ - \Lambda]. \quad (10)$$

When applying the Gaussian boundaries in (4) and (5) coordinatewise to each $W_\ell(\cdot)$, we obtain two variants of the SAGE boundary, (9) and (10), with widths of order $\mathcal{O}(\log \log n/n)$ and

$\mathcal{O}(\log n/n)$, respectively. The rate of $\Upsilon_{\alpha,m}(\cdot)$ in (9) matches the law of the iterated logarithm rate [14], since $\limsup_{n \rightarrow \infty} n|U_n - \theta|/\log \log n < \infty$ almost surely for canonical U -statistics.

Moreover, we note that the SAGE boundary proposed in Theorem 5 is a one-sided upper boundary. This is sufficient for many classical statistical inference based on degenerate U -statistics, including distributional tests based on MMD or energy distance, where evidence against the null is typically accumulated in the upper tail. We defer the lower boundary results to Section B.1 and focus on the upper boundary throughout the paper and the subsequent example.

In practice, implementation of the proposed SAGE boundaries requires consistent eigenvalue estimation, which we formalize in Assumption 1.

Assumption 1. *For a small $\iota > 0$, there exist consistent estimators $\widehat{\Lambda}$, $\widehat{\Lambda}^+$, $\widehat{\Lambda}_\beta^+$ and $\widehat{\Lambda}_{\beta,g}^+$ such that $|\widehat{\Lambda} - \Lambda| + |\widehat{\Lambda}^+ - \Lambda^+| + |\widehat{\Lambda}_\beta^+ - \Lambda_\beta^+| + |\widehat{\Lambda}_{\beta,g}^+ - \Lambda_{\beta,g}^+| = o_{a.s.}(n^{-\iota})$.*

Remark 1. *Assumption 1 is a high-level condition, and we provide an empirical eigenvalue procedure that satisfies this condition. Consider the centered Gram matrix*

$$\widehat{K}_n(i, j) := h(X_i, X_j) - U_n, \quad 1 \leq i, j \leq n.$$

One can let $(\widehat{\lambda}_{\ell,n})_{\ell \geq 1}$ be the eigenvalues of $n^{-1}\widehat{\mathbf{K}}_n$, in which the matrix $\widehat{\mathbf{K}}_n = \{\widehat{K}_n(i, j)\}_{i,j=1}^n$. For simplicity, we write $\widehat{\lambda}_\ell$ for $\widehat{\lambda}_{\ell,n}$ when no confusion arises. Define $\widehat{\Lambda} = n^{-1} \sum_{i=1}^n h(X_i, X_i) - U_n$, $\widehat{\Lambda}^+ = \sum_{\ell: \widehat{\lambda}_\ell > 0}^{L_n} \widehat{\lambda}_\ell$, $\widehat{\Lambda}_\beta^+ = \sum_{\ell: \widehat{\lambda}_\ell > 0}^{L_n} \widehat{\lambda}_\ell \log(1/\beta_\ell)$, and $\widehat{\Lambda}_{\beta,g}^+ = \sum_{\ell: \widehat{\lambda}_\ell > 0}^{L_n} \widehat{\lambda}_\ell \{g^{-1}(\alpha\beta_\ell)\}^2$, where the truncation number $L_n \asymp n^a$ and $\beta_\ell \asymp \ell^{-b}$ for some $0 < a < 1/2$ and $b > 1$. Results in related empirical operator analyses including [23, 34] and Weyl inequality ensure that Assumption 1 holds under regularity conditions. Further details are provided in Section B.2.

Theorem 6. *Under Assumption 1 and the conditions in Theorem 4-5, for any $\alpha \in (0, 1)$, $m \geq 1$,*

$$\liminf_{m \rightarrow \infty} \mathbb{P} \left(\forall n \geq m : U_n \leq \theta + \widehat{\Upsilon}_{\alpha,m}(n) \right) \geq 1 - \alpha,$$

where $\widehat{\Upsilon}_{\alpha,m}(n)$ can be chosen in either of the following two ways:

$$\widehat{\Upsilon}_{\alpha,m}^{LIL}(n) = \frac{(\eta^{1/4} + \eta^{-1/4})^2}{2n} \left[\left\{ s \log \log \left(\max \left\{ \frac{\eta n}{m}, e \right\} \right) + \log \frac{\zeta(s)}{\alpha(\log \eta)^s} \right\} \widehat{\Lambda}^+ + \widehat{\Lambda}_\beta^+ \right] - \frac{\widehat{\Lambda}}{n}, \quad (11)$$

$$\widehat{\Upsilon}_{\alpha,m}^{GM}(n) = \frac{1}{n} \left[\widehat{\Lambda}^+ \log \left(\frac{n}{m} \right) + \widehat{\Lambda}_{\beta,g}^+ - \widehat{\Lambda} \right]. \quad (12)$$

Theorem 6 provides the asymptotic coverage guarantee for the plug-in SAGE boundaries. The duality between CSs and sequential tests makes our framework well adapted for modern sequential testing and continuous monitoring. Formally, an asymptotic $(1 - \alpha)$ -CS $\{\mathcal{C}_n\}_{n \geq m}$ is equivalent to a family of asymptotic level- α sequential tests for $H_0 : \theta = \theta_0$. By defining the rejection rule as $\phi_n = \mathbf{1}\{\theta_0 \notin \mathcal{C}_n\}$, the Type I error is asymptotically controlled at level α for any stopping time.

Algorithm 1 Nondegenerate AsympCSs

Require: Data stream X_1, X_2, \dots ; symmetric kernel h ; level $\alpha \in (0, 1)$; delayed start $m \geq 2$.

Ensure: Two-sided $(1 - \alpha)$ -AsympCSs $(\mathcal{C}_n^{\text{ND}})_{n \geq m}$ for $\theta = \mathbb{E}h(X_1, X_2)$.

- 1: **for** $n = m, m + 1, \dots$ **do**
 - 2: Compute $U_n \leftarrow \binom{n}{2}^{-1} \sum_{1 \leq i < j \leq n} h(X_i, X_j)$.
 - 3: Compute boundary $\gamma_{\alpha, m}(\cdot)$ using (4) or (5) and estimate $\hat{\sigma}_n^2$ from (6).
 - 4: Output $\mathcal{C}_n^{\text{ND}} \leftarrow [U_n - 2\hat{\sigma}_n \gamma_{\alpha, m}(n), U_n + 2\hat{\sigma}_n \gamma_{\alpha, m}(n)]$.
 - 5: **end for**
-

Algorithm 2 Degenerate AsympCSs

Require: Data stream X_1, X_2, \dots ; canonical symmetric kernel h ; level $\alpha \in (0, 1)$; delayed start $m \geq 2$; truncation number L_n ; weights $(\beta_\ell)_{\ell \geq 1}$ with $\sum_{\ell \geq 1} \beta_\ell = 1$

Ensure: One-sided $(1 - \alpha)$ -AsympCSs $(\mathcal{C}_n^{\text{D}})_{n \geq m}$ for $\theta = \mathbb{E}h(X_1, X_2)$.

- 1: **for** $n = m, m + 1, \dots$ **do**
 - 2: Compute $U_n \leftarrow \binom{n}{2}^{-1} \sum_{1 \leq i < j \leq n} h(X_i, X_j)$.
 - 3: Form the centered Gram matrix $\hat{\mathbf{K}}_n \leftarrow h(X_i, X_j) - U_n, 1 \leq i, j \leq n$.
 - 4: Retain the top L_n eigenvalues of the scaled matrix $n^{-1} \hat{\mathbf{K}}_n$ in absolute value: $\hat{\lambda}_1, \dots, \hat{\lambda}_{L_n}$.
 - 5: Compute $\hat{\Lambda}, \hat{\Lambda}^+, \hat{\Lambda}_\beta^+, \hat{\Lambda}_{\beta, g}^+$ provided in Remark 1.
 - 6: Compute the SAGE boundary $\hat{\Upsilon}_{\alpha, m}(n)$ using (11) or (12).
 - 7: Output $\mathcal{C}_n^{\text{D}} \leftarrow [U_n - \hat{\Upsilon}_{\alpha, m}(n), \infty)$.
 - 8: **end for**
-

Implementation. Building upon theoretical guarantees established for both regimes, we provide two algorithmic templates for constructing these anytime-valid AsympCSs below:

A key practical consideration in implementing Algorithm 2 is the choice of the significance level allocation weights $(\beta_\ell)_{\ell \geq 1}$. To tighten the SAGE boundaries, a simple heuristic is to choose the allocation weights $(\beta_\ell)_{\ell \geq 1}$ to minimize Λ_β^+ under the constraints $\beta_\ell \geq 0$ and $\sum_{\ell \geq 1} \beta_\ell = 1$. Let $p_\ell = \max\{\lambda_\ell, 0\}/\Lambda^+$. Then,

$$\Lambda_\beta^+ = \sum_{\ell \geq 1} \max\{\lambda_\ell, 0\} \log(1/\beta_\ell) = \Lambda^+ \left\{ \sum_{\ell \geq 1} p_\ell \log(1/p_\ell) + \text{KL}(\mathbf{p} \parallel \boldsymbol{\beta}) \right\},$$

where the KL divergence $\text{KL}(\mathbf{p} \parallel \boldsymbol{\beta}) := \sum_{\ell \geq 1} p_\ell \log(p_\ell/\beta_\ell)$ is nonnegative and equals zero if and only if $\beta_\ell = p_\ell$ for all $\ell \geq 1$. Hence, the optimal choice is $\beta_\ell^* = \max\{\lambda_\ell, 0\}/\Lambda^+$, which motivates a data-driven choice $\hat{\beta}_\ell = \max\{\hat{\lambda}_\ell, 0\}/\hat{\Lambda}^+$ where $\hat{\Lambda}^+ = \sum_{\ell: \hat{\lambda}_\ell > 0} \hat{\lambda}_\ell$ for each $n = m, m + 1, \dots$

4 Examples

Here, we introduce four concrete examples, which are adopted in numerical experiments.

Sample variance. The target parameter $\theta = \text{Var}(X_1)$ is estimated by the kernel: $h(x, y) = (x - y)^2/2$. Let $\mu = \mathbb{E}X_1$. The first-order projection and its variance are given by:

$$h_1(x) = \{(x - \mu)^2 - \theta\} / 2, \quad \sigma^2 = \text{Var}\{(X_1 - \mu)^2\} / 4.$$

If $X_1 \sim \mathcal{N}(\mu, \theta)$, the fourth central moment is $3\theta^2$, which yields a closed-form variance $\sigma^2 = \theta^2/2$. Since Theorem 2 requires $\mathbb{E}h^4 < \infty$, the sample variance mandates an eighth-moment condition on X_1 , which explains its mild sensitivity to heavier-tailed data observed in our simulations.

Gini mean difference (GMD). The target $\theta = \mathbb{E}|X_1 - X_2|$ is associated with the kernel: $h(x, y) = |x - y|$. The first-order projection and its corresponding variance are defined as:

$$h_1(x) = \mathbb{E}|x - X_2| - \theta, \quad \sigma^2 = \text{Var}\{\mathbb{E}(|X_1 - X_2| \mid X_1)\}.$$

If $X_1 \sim \mathcal{N}(\mu, v)$, the target evaluates to $\theta = 2\sqrt{v/\pi}$, and the projection variance admits the exact form $\sigma^2 = v \{1/3 + (2\sqrt{3} - 4)/\pi\}$. A finite fourth moment on X_1 guarantees the asymptotic validity, making GMD more robust to heavy tails.

Spatial Kendall's tau. Consider bivariate data $\mathbf{X}_i = (X_{i1}, X_{i2})^\top \in \mathbb{R}^2$. The kernel for the off-diagonal entry of the two-dimensional spatial Kendall's tau matrix [4] is:

$$h(\mathbf{x}, \mathbf{y}) = \frac{(x_1 - y_1)(x_2 - y_2)}{\|\mathbf{x} - \mathbf{y}\|_2^2} \mathbf{1}\{\mathbf{x} \neq \mathbf{y}\}.$$

The target $\theta = \mathbb{E}\{h(\mathbf{X}_1, \mathbf{X}_2)\} \in [-1/2, 1/2]$ provides a robust measure of directional association between two coordinates. Under a bivariate elliptical distribution with shape correlation $\rho \in [-1, 1]$, the target has a closed form $\theta = (1 - \sqrt{1 - \rho^2}) / (2\rho)$ when $\rho \neq 0$. In our simulation, we set $\rho = 0.6$, which then gives $\theta = 1/6$. Further details are deferred to Appendix A.4. Since the kernel is bounded, all moment conditions required by Theorem 3 hold automatically, which explains the stable coverage observed in the heavy-tailed settings considered here.

MMD with Gaussian kernel. Let $\mathbf{Z}_i = (X_i, Y_i)^\top$ denote a paired observation where $X_i \sim P$ and $Y_i \sim Q$. The unbiased squared MMD statistic [16] employs the kernel:

$$h(\mathbf{z}, \mathbf{z}') = k(x, x') + k(y, y') - k(x, y') - k(x', y),$$

where $k(x, y) = \exp(-|x - y|^2/2)$ is the Gaussian kernel. The target parameter is $\theta = \mathbb{E}h(\mathbf{Z}_1, \mathbf{Z}_2) =: \text{MMD}^2(P, Q)$. The first-order projection is defined generally as $h_1(\mathbf{z}) = \mathbb{E}h(\mathbf{z}, \mathbf{Z}) - \theta$. Under the null hypothesis that $P = Q$, a direct calculation yields $\theta = 0$ and the projection vanishes: $\sigma^2 = \text{Var}\{h_1(\mathbf{Z})\} = 0$, then the U-statistic completely loses its first-order term and falls exactly into the canonical degenerate case.

5 Simulations

Non-degenerate case. For non-degenerate U-statistics, we consider GMD under three data generating distributions: the standard Gaussian, t_{10} and Laplace with density $f(x) = \exp(-\sqrt{2}|x|)/\sqrt{2}$. To evaluate the empirical coverage and the average width of the proposed AsympCSs, we conduct Monte Carlo simulations with 500 independent replications. We set the nominal error rate to $\alpha = 0.05$ throughout, and monitor the U-statistics continuously from a start $m = 400$ up to $n_{\max} = 10,000$.

We compare against the baseline **classical pointwise CIs** based on the asymptotic normality and evaluate two variants of the AsympCS in (7): **AsympCS-LIL** using the stitched boundary in (4) with $\eta = 2.0$ and $s = 1.4$ suggested by [20], and **AsympCS-GM** using the Gaussian-mixture boundary in (5). The results are illustrated in Figures 1 and A.2-A.3 in Appendix A.2. Additional simulation results for other U-statistics, including sample variance and Spatial Kendall’s tau, are deferred to Appendix A.4. As shown in the left panel of Figure 1, the classical CIs suffer from a severe loss of coverage due to repeated sequential evaluations; their cumulative miscoverage rate rapidly climbs above the nominal α level. In contrast, both AsympCS-GM and AsympCS-LIL maintain the miscoverage rate below α uniformly across the entire horizon. The plot of one sample path for U_n in the right panel of Figure 1 further illustrates how the valid AsympCSs safely envelop the true parameter.

The middle panel of Figure 1 traces the average half-widths of the proposed AsympCSs for GMD under the standard Gaussian distribution. As expected from theory, the AsympCSs are wider than the classical pointwise CIs, reflecting the necessary correction for continuous monitoring. Notably, although the AsympCS-GM boundary shrinks at the slower rate $\sqrt{\log n/n}$, it yields sharper intervals in the finite-sample situation. This observation is consistent with [20]: the GM boundary can be tighter at moderate sample sizes, but is eventually outperformed by the AsympCS-LIL boundary, which attains the asymptotically optimal $\sqrt{\log \log n/n}$ rate. A similar phenomenon also emerges in our degenerate experiments, translating into higher finite-sample power using the SAGE-GM boundary.

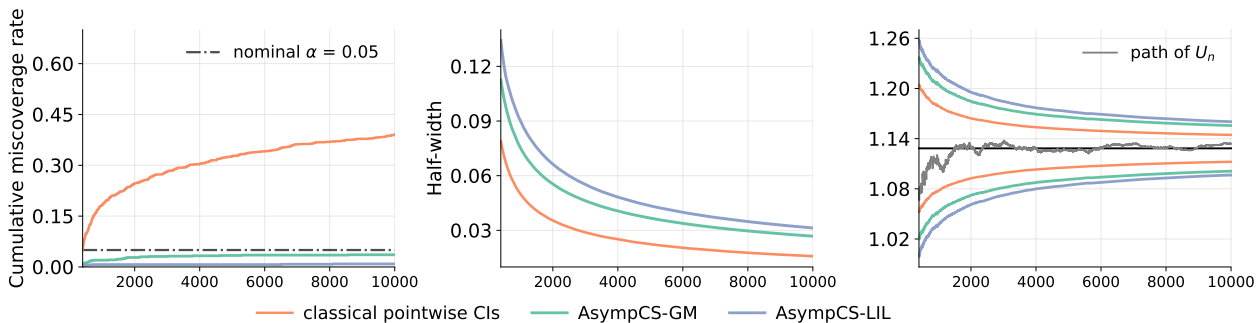


Figure 1: Left: cumulative miscoverage rates of the proposed AsympCSs and the classical pointwise CIs for GMD under the standard Gaussian distribution. Middle: averaged half-widths of the proposed AsympCSs and the classical pointwise CIs. Right: a single sample path of the statistics U_n for GMD alongside the three boundaries, where the black horizontal line indicates the true parameter. The horizontal axis in all three panels represents the sample size.

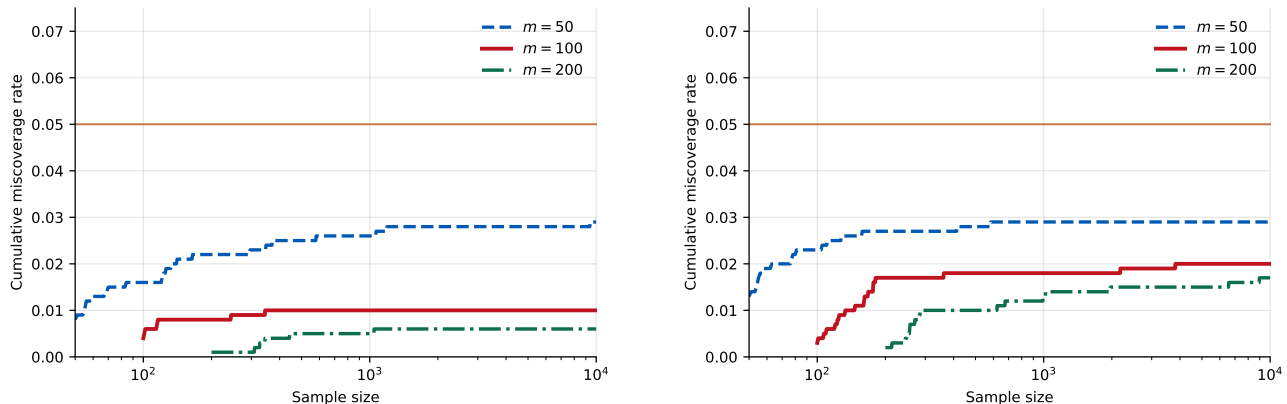


Figure 2: Sensitivity of AsympCS-LIL for GMD to the cold-start parameter $m \in \{50, 100, 200\}$. Cumulative miscoverage rates are reported under the standard Gaussian (left panel) and t_{10} (right panel) distributions.

Also we consider the sensitivity to the cold-start parameter m . We examine the reliability of the asymptotic coverage under continuous monitoring by varying the cold-start parameter $m \in \{50, 100, 200\}$. Figure 2 reports the cumulative miscoverage rates of the AsympCS-LIL for GMD under the standard Gaussian and the t_{10} distributions. In both settings, once the start time $m \geq 50$, the cumulative miscoverage rate remains below the level α for up to 10^4 observations. It shows that a moderate cold-start absorbs early finite-sample deviations.

Degenerate case. For degenerate U-statistics, we study two-sample sequential testing based on MMD with Gaussian kernel over the time horizon from $m = 400$ to $n_{\max} = 2,000$. The truncation number L_n is set to be $\lceil n^{1/4} \rceil$. We evaluate the sequential MMD test under the standard Gaussian null $H_0 : P = Q$ and under mean-shift alternatives $H_1 : P \neq Q$, parameterized by δ . We compare against the baseline **classical test** using quantiles of a centered weighted sum of chi-squared random variables as critical values, and employ the proposed SAGE boundaries in (11) and (12), denoted by **SAGE-LIL** and **SAGE-GM** respectively. All results are based on 500 independent Monte Carlo replications. Additional simulation results under other null distributions are deferred to Appendix A.3.

As shown in the left panel of Figure 3, the classical testing rule completely fails under continuous monitoring, with its empirical rejection rate rapidly accumulating beyond the nominal α level. In contrast, the SAGE boundaries yield sizes close to zero under H_0 , while their power approaches one as the sample size increases under H_1 where $\delta = 0.3$ in the simulation. It confirms that our framework achieves rigid Type I error control and has enough power simultaneously. The right panel of Figure 3 also visualizes the underlying mechanism via a single sample path under the null.

To examine the sensitivity to signal strength, we evaluate the power over a grid of mean shifts $\delta \in [0, 0.45]$ at the fixed sample size $n = 2000$. As depicted in the middle panel of Figure 3, the empirical power based on our SAGE boundaries increases from zero to one, demonstrating their effectiveness for sequential testing.

The empirical performance of the sequential test relies on the significance level budget

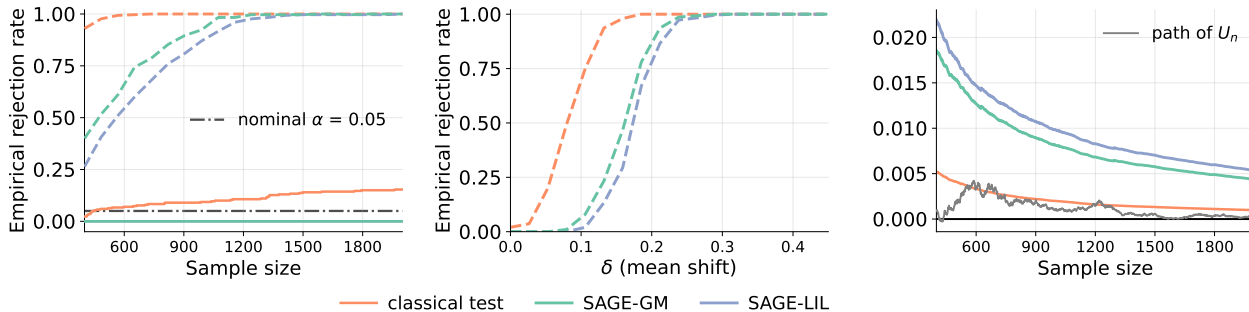


Figure 3: Left: the size and power comparison of the proposed sequential testing procedure using the SAGE boundaries and the classical test procedure for sequential two-sample test with MMD kernel statistics under standard Gaussian distribution. Dashed lines represent the power under H_1 with $\delta = 0.3$, while solid lines represent the size under H_0 with $\delta = 0$. Middle: the empirical power over mean shifts $\delta \in [0, 0.45]$ at sample size $n = 2000$. Right: a single sample path of the MMD test statistic U_n alongside the three boundaries under H_0 .

allocation across the infinite eigenvalue spectrum. We compared various allocation strategies, including polynomial decay weights $\beta_\ell = \ell^{-b}/\zeta(b)$, exponential decay weights $\beta_\ell = (1 - e^{-c})e^{-c(\ell-1)}$, and our data-driven weights $\beta_\ell \propto \max\{\hat{\lambda}_\ell, 0\} / \hat{\Lambda}^+$, as shown in Figure A.1 in Appendix A.1. These results highlight the theoretical role of $\log(1/\beta_\ell)$: a larger b concentrates the budget on the leading eigenvalues and thus widens the boundary, while a larger c inflates the boundary through the rapid tail growth of $\log(1/\beta_\ell)$. Remarkably, the proposed data-driven procedure optimally distributes the budget, yielding the tightest boundary while remaining below the nominal level. This justifies our adoption of this data-driven approach to compute β_ℓ throughout the degenerate sequential testing experiments.

6 Concluding remarks

This paper develops asymptotic anytime-valid inference for degree-two U-statistics under continuous monitoring. In the nondegenerate regime, Hoeffding’s decomposition reduces the problem to the first-order projection, leading to AsympCS with LIL scale $\sqrt{\log \log n/n}$. In the degenerate regime, the limit is instead a spectral quadratic Gaussian chaos with unknown signed eigenvalues. The proposed SAGE boundary separates probability calibration from spectral estimation and yields a one-sided plug-in AsympCSs with the sharper $\log \log n/n$ scale under a weighted spectral approximation condition, covering degenerate kernel and distance-based tests.

Several limitations remain. The theory is restricted to scalar degree-two U-statistics; vector- or matrix-valued extensions require simultaneous time-uniform approximations and control of dimension-dependent errors, especially for spatial Kendall matrices and high-dimensional elliptical models [4, 12, 18]. The algorithms are not yet streaming-optimized, since exact updates, pairwise storage, and repeated eigendecompositions are costly; scalable versions may need incomplete U-statistics, incremental summaries, randomized low-rank updates, or linear-time

kernel approximations [16, 43, 5]. Finally, the degenerate theory assumes a verified spectral approximation rate, and finite-sample cold starts, local degeneracy, and automatic switching between regimes remain open.

References

- [1] Miguel A. Arcones and Evarist Giné. Limit theorems for U-processes. *The Annals of Probability*, 21(3):1494–1542, 1993.
- [2] Ludwig Baringhaus and Carsten Franz. On a new multivariate two-sample test. *Journal of Multivariate Analysis*, 88(1):190–206, 2004.
- [3] Cooper Boniece, Lajos Horvath, and Lorenzo Trapani. Sequential monitoring for distributional changepoint using degenerate U-statistics, 2025.
- [4] Kyungmee Choi and John I. Marden. A multivariate version of kendall’s tau. *Journal of Nonparametric Statistics*, 9(3):261–293, 1998.
- [5] Kacper Chwialkowski, Aaditya Ramdas, Dino Sejdinovic, and Arthur Gretton. Fast two-sample testing with analytic representations of probability measures. In *Advances in Neural Information Processing Systems 28*, 2015.
- [6] D. A. Darling and Herbert Robbins. Iterated logarithm inequalities. *Proceedings of the National Academy of Sciences of the United States of America*, 57(5):1188–1192, 1967.
- [7] Piet de Jong. A central limit theorem for generalized quadratic forms. *Probability Theory and Related Fields*, 75(2):261–277, 1987.
- [8] Victor H. de la Peña and Evarist Giné. *Decoupling: From Dependence to Independence*. Springer, New York, 1999.
- [9] Herold Dehling, Manfred Denker, and Walter Philipp. Invariance principles for von Mises and U-statistics. *Zeitschrift für Wahrscheinlichkeitstheorie und Verwandte Gebiete*, 67(2):139–167, 1984.
- [10] Herold Dehling, Roland Fried, Isabel García, and Martin Wendler. Change-point detection under dependence based on two-sample U-statistics. In *Asymptotic Laws and Methods in Stochastics*, volume 76 of *Fields Institute Communications*, pages 195–220. Springer, New York, 2015.
- [11] Herold Dehling, Kata Vuk, and Martin Wendler. Change-point detection based on weighted two-sample U-statistics. *Electronic Journal of Statistics*, 16(1):862–891, 2022.
- [12] Alexander Dürre, David E. Tyler, and Daniel Vogel. On the eigenvalues of the spatial sign covariance matrix in more than two dimensions. *Statistics & Probability Letters*, 111:80–85, 2016.
- [13] Dietmar Ferger. A functional law of the iterated logarithm for U-statistic type processes. *Acta Applicandae Mathematicae*, 78:115–120, 2003.
- [14] Evarist Giné, Stanisław Kwapien, Rafał Łatała, and Joel Zinn. The LIL for canonical U-statistics of order 2. *The Annals of Probability*, 29(1):520–557, 2001.

- [15] Felix Gnettner and Claudia Kirch. A new and flexible class of sharp asymptotic time-uniform confidence sequences. *Statistics & Probability Letters*, 226:110462, 2025.
- [16] Arthur Gretton, Karsten M. Borgwardt, Malte J. Rasch, Bernhard Schölkopf, and Alexander J. Smola. A kernel two-sample test. *Journal of Machine Learning Research*, 13:723–773, 2012.
- [17] Peter Hall. On the invariance principle for U-statistics. *Stochastic Processes and their Applications*, 9(2):163–174, 1979.
- [18] Fang Han and Han Liu. ECA: High-dimensional elliptical component analysis in non-gaussian distributions. *Journal of the American Statistical Association*, 113(521):252–268, 2018.
- [19] Wassily Hoeffding. A class of statistics with asymptotically normal distribution. *The Annals of Mathematical Statistics*, 19(3):293–325, 1948.
- [20] Steven R. Howard, Aaditya Ramdas, Jon McAuliffe, and Jasjeet Sekhon. Time-uniform, nonparametric, nonasymptotic confidence sequences. *The Annals of Statistics*, 49(2):1055–1080, 2021.
- [21] Maurice G. Kendall. A new measure of rank correlation. *Biometrika*, 30(1/2):81–93, 1938.
- [22] Claudia Kirch and Christina Stoehr. Sequential change point tests based on U-statistics. *Scandinavian Journal of Statistics*, 49(3):1184–1214, 2022.
- [23] Vladimir Koltchinskii and Evarist Giné. Random matrix approximation of spectra of integral operators. *Bernoulli*, 6(1):113–167, 2000.
- [24] Vladimir S. Korolyuk and Yuri V. Borovskich. *Theory of U-Statistics*. Kluwer Academic Publishers, Dordrecht, 1994.
- [25] Alan J. Lee. *U-Statistics: Theory and Practice*. Marcel Dekker, New York, 1990.
- [26] Weijia Li, Leheng Cai, and Qirui Hu. Strong Gaussian approximation for U-statistics in high dimensions and beyond. *arXiv preprint arXiv:2603.10595*, 2026.
- [27] Henry B. Mann and Donald R. Whitney. On a test of whether one of two random variables is stochastically larger than the other. *The Annals of Mathematical Statistics*, 18(1):50–60, 1947.
- [28] Nitis Mukhopadhyay and Inger Vik. Asymptotic results for stopping times based on U-statistics. *Sequential Analysis*, 4(1–2):83–109, 1985.
- [29] Nitis Mukhopadhyay and Inger Vik. Convergence rates for two-stage confidence intervals based on U-statistics. *Annals of the Institute of Statistical Mathematics*, 40(1):111–117, 1988.
- [30] Masoud M. Nasari. Studentized processes of U-statistics, 2009.
- [31] Aaditya Ramdas, Peter Grünwald, Vladimir Vovk, and Glenn Shafer. Game-theoretic statistics and safe anytime-valid inference. *Statistical Science*, 38(4):576–601, 2023.
- [32] Herbert Robbins. Statistical methods related to the law of the iterated logarithm. *The Annals of Mathematical Statistics*, 41(5):1397–1409, 1970.

- [33] Herbert Robbins and David Siegmund. Boundary crossing probabilities for the Wiener process and sample sums. *The Annals of Mathematical Statistics*, 41(5):1410–1429, 1970.
- [34] Lorenzo Rosasco, Mikhail Belkin, and Ernesto De Vito. On learning with integral operators. *Journal of Machine Learning Research*, 11:905–934, 2010.
- [35] Dino Sejdinovic, Bharath Sriperumbudur, Arthur Gretton, and Kenji Fukumizu. Equivalence of distance-based and RKHS-based statistics in hypothesis testing. *The Annals of Statistics*, 41(5):2263–2291, 2013.
- [36] Robert J. Serfling. *Approximation Theorems of Mathematical Statistics*. John Wiley & Sons, New York, 1980.
- [37] Raymond N. Sproule. Sequential nonparametric fixed-width confidence intervals for U-statistics. *The Annals of Statistics*, 13(1):228–235, 1985.
- [38] Gábor J. Székely and Maria L. Rizzo. Energy statistics: A class of statistics based on distances. *Journal of Statistical Planning and Inference*, 143(8):1249–1272, 2013.
- [39] Gábor J. Székely, Maria L. Rizzo, and Nail K. Bakirov. Measuring and testing dependence by correlation of distances. *The Annals of Statistics*, 35(6):2769–2794, 2007.
- [40] Jean Ville. *Étude Critique de la Notion de Collectif*. Gauthier-Villars, Paris, 1939.
- [41] Ian Waudby-Smith, David Arbour, Ritwik Sinha, Edward H. Kennedy, and Aaditya Ramdas. Time-uniform central limit theory and asymptotic confidence sequences. *The Annals of Statistics*, 52(6):2613–2640, 2024.
- [42] Ian Waudby-Smith and Aaditya Ramdas. Estimating means of bounded random variables by betting. *Journal of the Royal Statistical Society Series B: Statistical Methodology*, 86(1):1–27, 02 2024.
- [43] Wojciech Zaremba, Arthur Gretton, and Matthew B. Blaschko. B-test: A non-parametric, low variance kernel two-sample test. In *Advances in Neural Information Processing Systems 26*, pages 755–763, 2013.

A Additional numerical results

A.1 Results of sensitivity experiments

Figure A.1 reports the sensitivity analysis for the weight allocation, as discussed in Section 5. The results show that using predefined deterministic weights, such as polynomial allocations $\beta_\ell \propto \ell^{-b}$ with a large value of b , can lead to overly conservative boundaries. To improve efficiency, the data-driven allocation suggests choosing weights proportional to the positive part of the spectrum, namely $\beta_\ell^* \propto \max\{\lambda_\ell, 0\}$. Since the population spectrum is unknown, in our simulations we adopt the dynamically updated plug-in weights $\hat{\beta}_{\ell,n} \propto \max\{\hat{\lambda}_{\ell,n}, 0\}$.

We note a minor but important technical distinction between the theoretical SAGE boundary in Theorem 6 and its practical implementation in the simulations. In the theorem, the weights are required to be a fixed deterministic nonnegative array satisfying $\sum_{\ell \geq 1} \beta_{\ell,n} = 1$, which ensures the time-uniform union bound

$$\mathbb{P}\left(\bigcup_{\ell \geq 1} E_\ell^c\right) \leq \sum_{\ell \geq 1} \alpha \beta_{\ell,n} = \alpha.$$

By contrast, the simulation procedure uses the data-driven weights $\hat{\beta}_{\ell,n}$, which are random. Thus, this implementation should be viewed as an empirical plug-in heuristic. As shown in Figure A.1, this heuristic empirically maintains nominal coverage and delivers robust practical performance. Providing a rigorous time-uniform validity theory for SAGE boundaries with dynamically updated random weights is an interesting direction for future work.

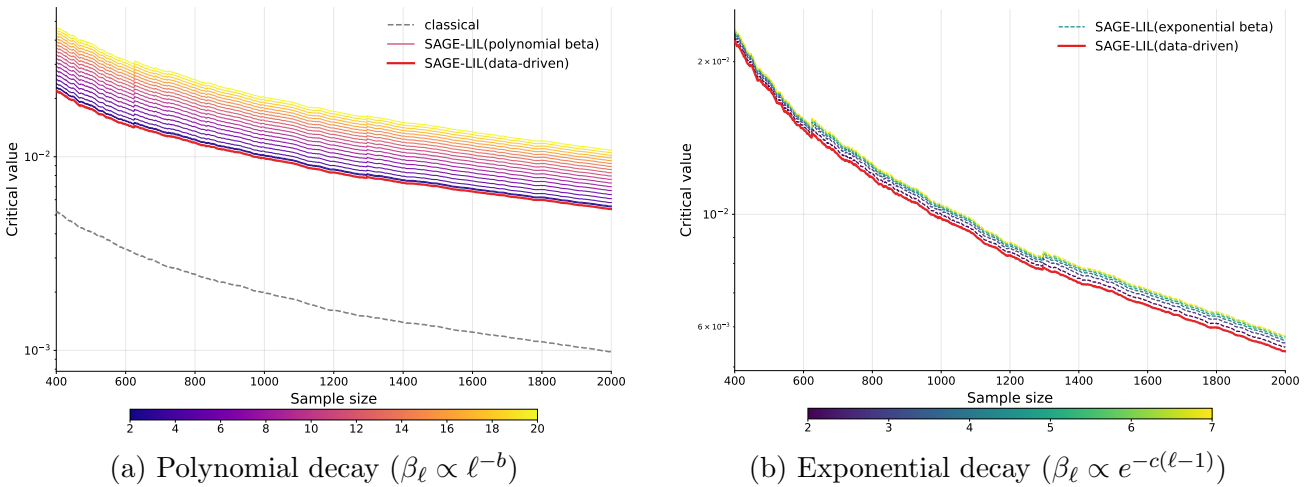


Figure A.1: Sensitivity of the width of SAGE-LIL to the spectral weight allocation β_ℓ . The colorbars indicate the decay-rate parameters: the polynomial degree $b \in [2, 20]$ in panel (a), and the exponential rate $c \in [2, 7]$ in panel (b).

A.2 AsympCSs for GMD under Laplace and t_{10} distributions

Figures A.2-A.3 present the performance of the proposed AsympCSs for GMD under Laplace and t_{10} distributions. In our implementation, the data dimension is set to $d = 1$ for the GMD, sample variance, and MMD tests, and $d = 2$ for the Spatial Kendall's tau.

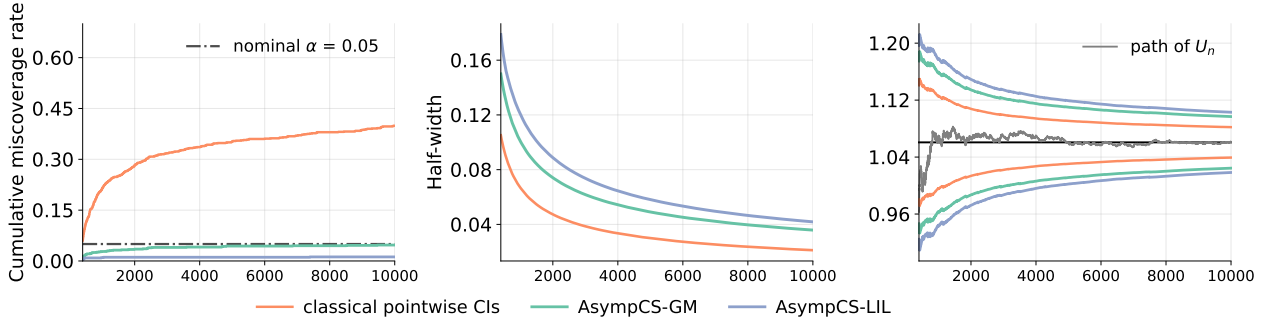


Figure A.2: Left: cumulative miscoverage rates of the proposed AsympCSs and the classical pointwise CIs for GMD under the Laplace distribution. Middle: averaged half-widths of the proposed AsympCSs and the classical pointwise CIs. Right: a single sample path of the statistics U_n for GMD alongside the three boundaries, where the black horizontal line indicates the true parameter. The horizontal axis in all three panels represents the sample size.

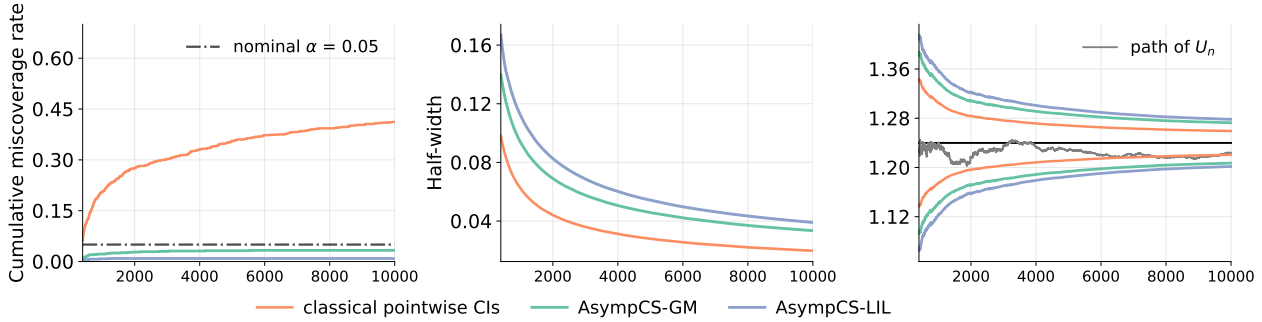


Figure A.3: Left: cumulative miscoverage rates of the proposed AsympCSs and the classical pointwise CIs for GMD under the t_{10} distribution. Middle: averaged half-widths of the proposed AsympCSs and the classical pointwise CIs. Right: a single sample path of the statistics U_n for GMD alongside the three boundaries, where the black horizontal line indicates the true parameter. The horizontal axis in all three panels represents the sample size.

A.3 Two-sample sequential testing based on MMD under Laplace and t_{10} null distributions

Figures A.4-A.5 present the performance of the sequential testing procedures using the proposed SAGE boundaries for sequential two-sample test with MMD kernel statistics under Laplace and t_{10} distributions.

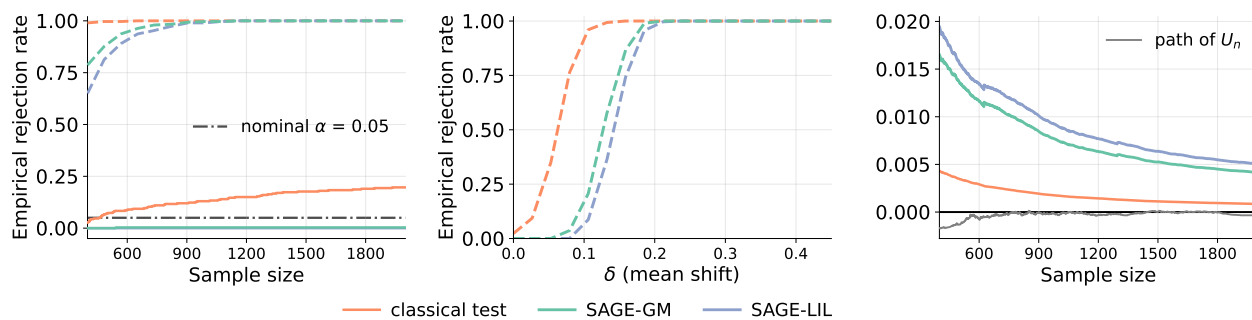


Figure A.4: Left: the size and power comparison of the proposed sequential testing procedure using the SAGE boundaries and the classical test procedure for sequential two-sample test with MMD kernel statistics under Laplace distribution. Dashed lines represent the power under H_1 with $\delta = 0.3$, while solid lines represent the size under H_0 with $\delta = 0$. Middle: the empirical power over mean shifts $\delta \in [0, 0.45]$ at sample size $n = 2000$. Right: a single sample path of the MMD test statistic U_n alongside the three boundaries under H_0 .

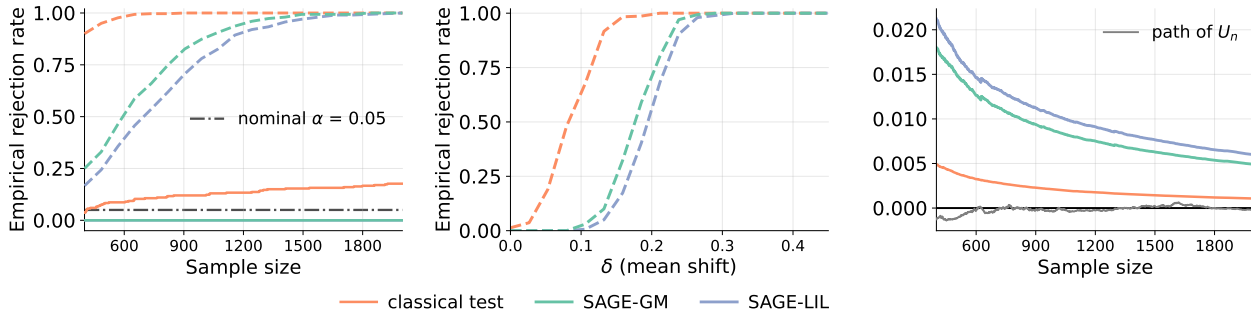


Figure A.5: Left: the size and power comparison of the proposed sequential testing procedure using the SAGE boundaries and the classical test procedure for sequential two-sample test with MMD kernel statistics under t_{10} distribution. Dashed lines represent the power under H_1 with $\delta = 0.3$, while solid lines represent the size under H_0 with $\delta = 0$. Middle: the empirical power over mean shifts $\delta \in [0, 0.45]$ at sample size $n = 2000$. Right: a single sample path of the MMD test statistic U_n alongside the three boundaries under H_0 .

A.4 Additional experiments

Figures A.6-A.8 present the performance of the proposed AsympCSs for sample variance under the same three distributions as in Section 5.

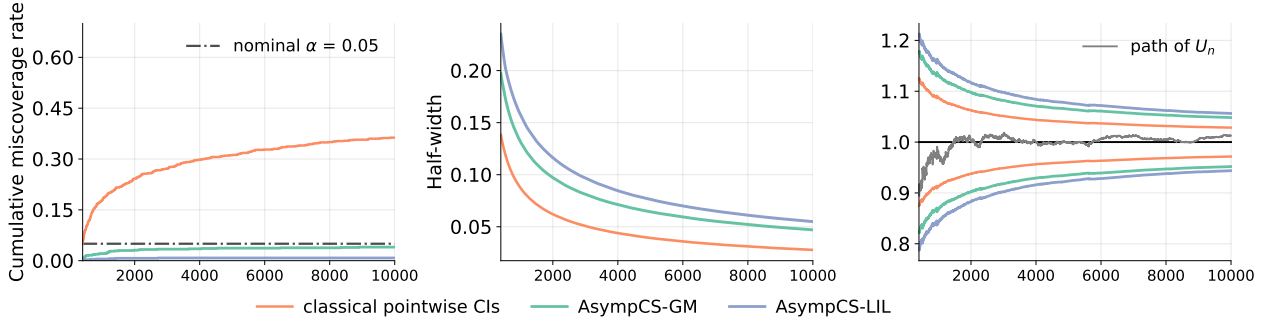


Figure A.6: Left: cumulative miscoverage rates of the proposed AsympCSs and the classical pointwise CIs for sample variance under the Gaussian distribution. Middle: averaged half-widths of the proposed AsympCSs and the classical pointwise CIs. Right: a single sample path of the statistics U_n for sample variance alongside the three boundaries, where the black horizontal line indicates the true parameter. The horizontal axis in all three panels represents the sample size.

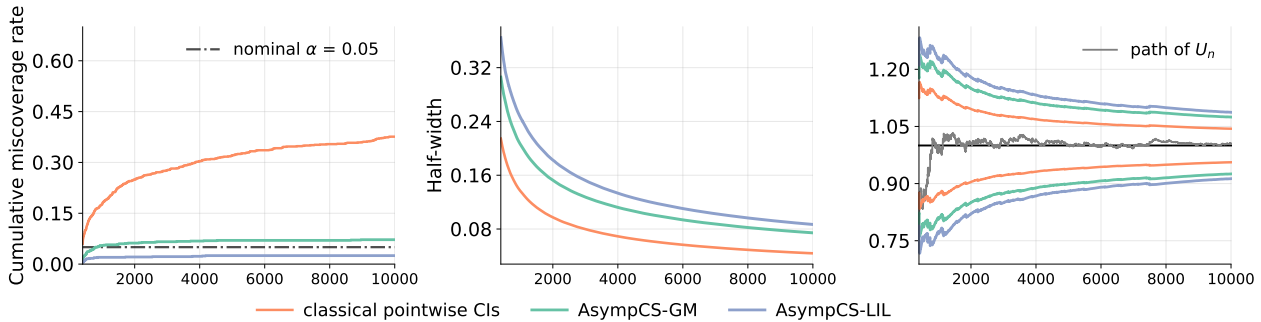


Figure A.7: Left: cumulative miscoverage rates of the proposed AsympCSs and the classical pointwise CIs for sample variance under the Laplace distribution. Middle: averaged half-widths of the proposed AsympCSs and the classical pointwise CIs. Right: a single sample path of the statistics U_n for sample variance alongside the three boundaries, where the black horizontal line indicates the true parameter. The horizontal axis in all three panels represents the sample size.

We notice that in Figures A.7-A.8, the cumulative miscoverage rate of AsympCS-GM slightly exceeds the nominal level. Theoretically, the Gaussian approximation errors for U_n and the consistency of the variance estimator $\hat{\sigma}_n^2$ depend on higher-order moments of the kernel. For the sample variance, such moment dependence is more pronounced, so heavier-tailed distributions require larger sample sizes for the asymptotic approximation to become accurate. Increasing the cold-start parameter m mitigates this finite-sample under-coverage by delaying monitoring until sufficient data have accumulated.

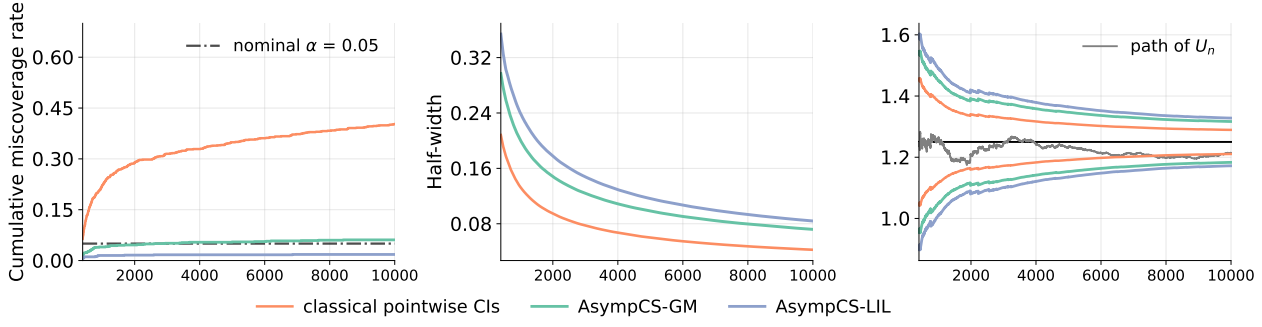


Figure A.8: Left: cumulative miscoverage rates of the proposed AsympCSs and the classical pointwise CIs for sample variance under the t_{10} distribution. Middle: averaged half-widths of the proposed AsympCSs and the classical pointwise CIs. Right: a single sample path of the statistics U_n for sample variance alongside the three boundaries, where the black horizontal line indicates the true parameter. The horizontal axis in all three panels represents the sample size.

Figures A.9-A.11 present the performance of the proposed AsympCSs estimation for Spatial Kendall's tau under the three distributions. Here, we detail the data generation process for the Spatial Kendall's tau estimation. Unlike the other three kernels we adopted, which utilize one-dimensional data drawn from the three specified distributions, Spatial Kendall's tau requires bivariate observations. To accommodate this, we generate two-dimensional data vectors $\mathbf{X}_i = (X_{i1}, X_{i2})^\top \in \mathbb{R}^2$ with a correlation structure. Specifically, the dependence is governed by a shape matrix Σ , defined as:

$$\Sigma = \begin{pmatrix} 1 & \rho \\ \rho & 1 \end{pmatrix}.$$

Throughout our simulations, the shape correlation is set to $\rho = 0.6$. For the two-dimensional elliptical distributions, \mathbf{X}_i has the scale mixture of normals representation:

$$\mathbf{X}_i = \sqrt{W_i} \mathbf{A} \mathbf{Z}_i, \quad (13)$$

where $\mathbf{Z}_i \sim \mathcal{N}(\mathbf{0}, \mathbf{I}_2)$ is a standard two-dimensional Gaussian vector, and \mathbf{A} is the Cholesky factor satisfying $\mathbf{A} \mathbf{A}^\top = \Sigma$. The multiplier $W_i > 0$ is a scalar random variable, independent of \mathbf{Z}_i , that dictates the tail heaviness of the resulting bivariate distribution.

In our simulations, we use three different W_i :

- **Gaussian:** $W_i = 1$ a.s., yielding the bivariate normal distribution with correlation ρ .
- **Student's t_{10} :** $W_i = \nu/V_i$, where $V_i \sim \chi_\nu^2$ with degrees of freedom $\nu = 10$.
- **Laplace:** $W_i \sim \text{Exp}(1)$, which generates the bivariate symmetric Laplace distribution.

Based on this representation, we first sample the standard two-dimensional Gaussian data \mathbf{Z}_i and obtain \mathbf{X}_i from (13), then compute the corresponding U-statistics. By mathematical derivation,

$$\theta = \mathbb{E} \left\{ \frac{(X_{11} - X_{21})(X_{12} - X_{22})}{\|\mathbf{X}_1 - \mathbf{X}_2\|_2^2} \mathbf{1}_{\{\mathbf{X}_1 \neq \mathbf{X}_2\}} \right\} = (1 - \sqrt{1 - \rho^2}) / (2\rho).$$

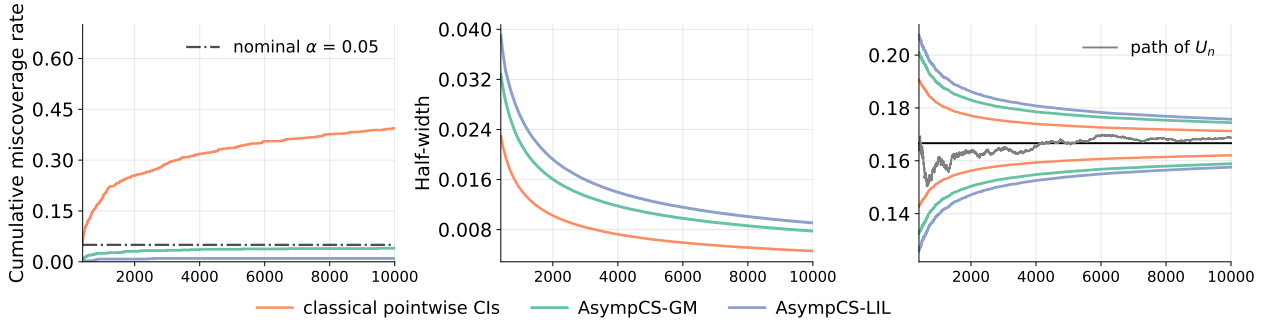


Figure A.9: Left: cumulative miscoverage rates of the proposed AsympCSs and the classical pointwise CIs for Spatial Kendall's tau under the Gaussian distribution. Middle: averaged half-widths of the proposed AsympCSs and the classical pointwise CIs. Right: a single sample path of the statistics U_n for Spatial Kendall's tau alongside the three boundaries, where the black horizontal line indicates the true parameter. The horizontal axis in all three panels represents the sample size.

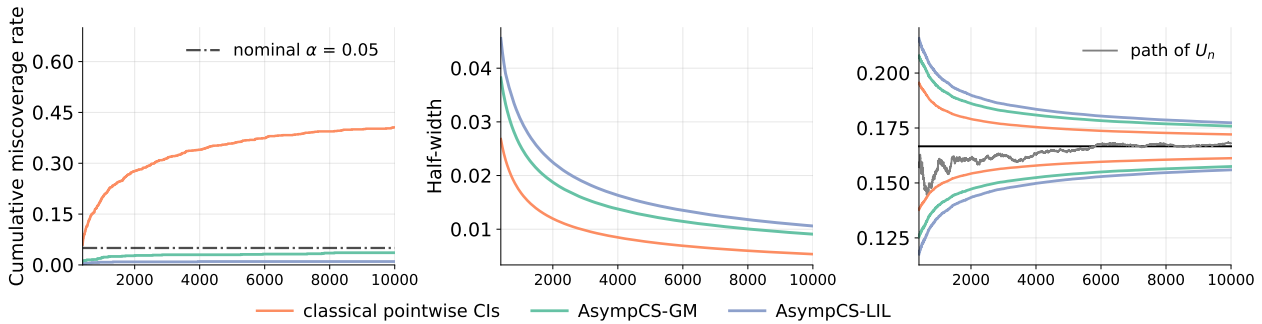


Figure A.10: Left: cumulative miscoverage rates of the proposed AsympCSs and the classical pointwise CIs for Spatial Kendall's tau under the Laplace distribution. Middle: averaged half-widths of the proposed AsympCSs and the classical pointwise CIs. Right: a single sample path of the statistics U_n for Spatial Kendall's tau alongside the three boundaries, where the black horizontal line indicates the true parameter. The horizontal axis in all three panels represents the sample size.

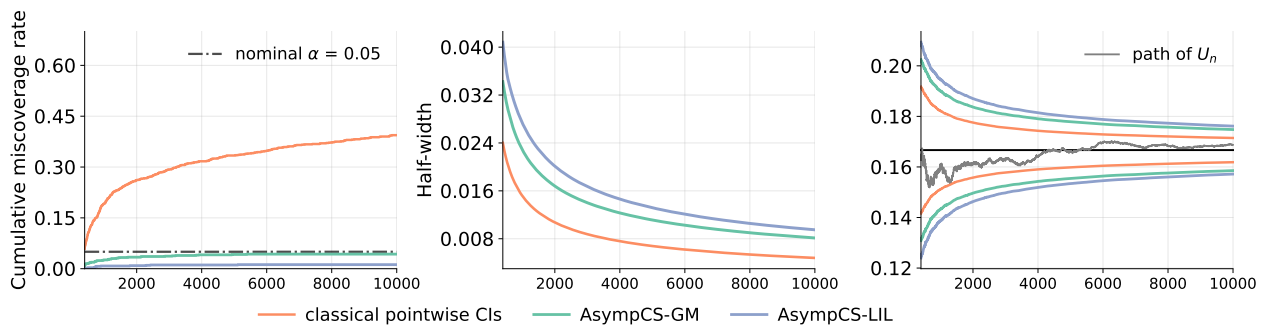


Figure A.11: Left: cumulative miscoverage rates of the proposed AsympCSs and the classical pointwise CIs for Spatial Kendall's tau under the t_{10} distribution. Middle: averaged half-widths of the proposed AsympCSs and the classical pointwise CIs. Right: a single sample path of the statistics U_n for Spatial Kendall's tau alongside the three boundaries, where the black horizontal line indicates the true parameter. The horizontal axis in all three panels represents the sample size.

A.5 Discussion of computational complexity

Algorithm 2 requires an eigen-decomposition of an $n \times n$ Gram matrix at each monitoring time, leading to a per-step computational cost of $\mathcal{O}(n^3)$. To reduce this cost, one may approximate the eigenvalues using an $N_n \times N_n$ sub-Gram matrix formed from the first $N_n = \lceil n^\varpi \rceil$ observations, where $\varpi \in (0, 1)$. For example, taking $\varpi = 2/3$ reduces the eigen-decomposition cost to $\mathcal{O}(N_n^3) = \mathcal{O}(n^2)$. Under the empirical estimation of eigenvalues discussed in Remark 1, this subsampling strategy still preserves the asymptotic anytime-validity of the resulting plug-in SAGE boundary, provided that the truncation number $L_n \asymp n^a$ with $0 < a < 1/3$.

B Further discussion

B.1 Discussion on the lower boundaries

Recall that $\Lambda = \sum_{\ell \geq 1} \lambda_\ell$. Define $\Lambda^- = \sum_{\ell: \lambda_\ell < 0} \lambda_\ell$, $\Lambda_\beta^- = \sum_{\ell: \lambda_\ell < 0} \lambda_\ell \log(1/\beta_\ell)$ and $\Lambda_{\beta, g}^- = \sum_{\ell: \lambda_\ell < 0} \lambda_\ell \{g^{-1}(\alpha\beta_\ell)\}^2$, where $g(a) = 2\{1 - \Phi(a) + a\phi(a)\}$. We now introduce the lower boundary $\mathcal{L}_{\alpha, m}(\cdot)$. Suppose that $\sum_{\ell \geq 1} |\lambda_\ell| < \infty$, $\Lambda_\beta^- < \infty$ and $\{W_\ell(\cdot)\}_{\ell \geq 1}$ are independent standard Brownian motions. For any $\alpha \in (0, 1)$, $m \geq 1$,

$$\mathbb{P} \left(\forall n \geq m : \frac{1}{n^2} \sum_{\ell \geq 1} \lambda_\ell \{W_\ell^2(n) - n\} \geq \mathcal{L}_{\alpha, m}(n) \right) \geq 1 - \alpha,$$

where $\mathcal{L}_{\alpha, m}(n)$ can be chosen in either of the following two ways:

$$\mathcal{L}_{\alpha, m}^{\text{LIL}}(n) = \frac{(\eta^{1/4} + \eta^{-1/4})^2}{2n} \left[\left\{ s \log \log \left(\max \left\{ \frac{\eta n}{m}, e \right\} \right) + \log \frac{\zeta(s)}{\alpha (\log \eta)^s} \right\} \Lambda^- + \Lambda_\beta^- \right] - \frac{\Lambda}{n},$$

$$\mathcal{L}_{\alpha, m}^{\text{GM}}(n) = \frac{1}{n} \left[\Lambda^- \log \left(\frac{n}{m} \right) + \Lambda_{\beta, g}^- - \Lambda \right].$$

If the kernel is positive semi-definite, then all eigenvalues are nonnegative, so the SAGE lower boundary degenerates to the deterministic term $\mathcal{L}_{\alpha, m}^{\text{LIL}}(n) = \mathcal{L}_{\alpha, m}^{\text{GM}}(n) = -\Lambda/n$.

B.2 Discussion on Remark 1

Let $\mathcal{K} : L^2(\mathbb{P}) \rightarrow L^2(\mathbb{P})$ be the integral operator induced by the centered kernel

$$K(x, y) := h(x, y) - \theta,$$

that is,

$$(\mathcal{K}f)(x) = \int K(x, y) f(y) d\mathbb{P}(y) = \mathbb{E}\{[h(x, X) - \theta]f(X)\}.$$

Let $(\lambda_\ell)_{\ell \geq 1}$ denote the eigenvalues of \mathcal{K} .

Given the sample X_1, \dots, X_n , define the empirical operator $\tilde{\mathcal{K}}_n$ by

$$(\tilde{\mathcal{K}}_n f)(x) = \frac{1}{n} \sum_{j=1}^n \{h(x, X_j) - \theta\} f(X_j).$$

Equivalently, when restricted to the sample points, $\tilde{\mathcal{K}}_n$ is represented by the matrix $n^{-1}\tilde{\mathbf{K}}_n$, where

$$\tilde{K}_n(i, j) := h(X_i, X_j) - \theta, \quad 1 \leq i, j \leq n.$$

Let $(\tilde{\lambda}_{\ell, n})_{\ell \geq 1}$ be the eigenvalues of $n^{-1}\tilde{\mathbf{K}}_n$.

Similarly, consider the centered Gram matrix

$$\hat{K}_n(i, j) := h(X_i, X_j) - U_n, \quad 1 \leq i, j \leq n,$$

and let $(\hat{\lambda}_{\ell, n})_{\ell \geq 1}$ be the eigenvalues of $n^{-1}\hat{\mathbf{K}}_n$. Then

$$n^{-1}\hat{\mathbf{K}}_n = n^{-1}\tilde{\mathbf{K}}_n - n^{-1}(U_n - \theta)\mathbf{J}_n,$$

where \mathbf{J}_n denotes the $n \times n$ all-ones matrix. Since $n^{-1}\mathbf{J}_n$ has eigenvalues $1, 0, \dots, 0$,

$$\|n^{-1}(U_n - \theta)\mathbf{J}_n\|_{\text{op}} = |U_n - \theta| = \mathcal{O}_{a.s.}\left(\frac{\log \log n}{n}\right).$$

By Weyl's inequality,

$$\sup_{\ell \geq 1} \left| \hat{\lambda}_{\ell, n} - \tilde{\lambda}_{\ell, n} \right| \leq |U_n - \theta| = \mathcal{O}_{a.s.}\left(\frac{\log \log n}{n}\right).$$

Moreover, by the results in [23, 34] under standard regularity conditions on the kernel function $h(\cdot, \cdot)$,

$$\|\tilde{\mathcal{K}}_n - \mathcal{K}\|_{\text{op}} = \mathcal{O}_{a.s.}\left(\sqrt{\frac{\log n}{n}}\right).$$

Again by Weyl's inequality,

$$\sup_{\ell \geq 1} \left| \tilde{\lambda}_{\ell, n} - \lambda_\ell \right| \leq \|\tilde{\mathcal{K}}_n - \mathcal{K}\|_{\text{op}} = \mathcal{O}_{a.s.}\left(\sqrt{\frac{\log n}{n}}\right).$$

Consequently,

$$\sup_{\ell \geq 1} \left| \hat{\lambda}_{\ell, n} - \lambda_\ell \right| = \mathcal{O}_{a.s.}\left(\sqrt{\frac{\log n}{n}}\right).$$

Let $x_+ = \max\{x, 0\}$ and define $\Lambda^+ = \sum_{\ell \geq 1} (\lambda_\ell)_+$ and $\Lambda_\beta^+ = \sum_{\ell \geq 1} \log(1/\beta_\ell) (\lambda_\ell)_+$, and their truncated empirical counterparts $\hat{\Lambda}^+ = \sum_{\ell=1}^{L_n} (\hat{\lambda}_\ell)_+$, $\hat{\Lambda}_\beta^+ = \sum_{\ell=1}^{L_n} \log(1/\beta_\ell) (\hat{\lambda}_\ell)_+$.

A sufficient condition for

$$\widehat{\Lambda}^+ - \Lambda^+ = \mathcal{O}_{a.s.}(n^{-\iota}), \quad \widehat{\Lambda}_\beta^+ - \Lambda_\beta^+ = \mathcal{O}_{a.s.}(n^{-\iota}), \quad \widehat{\Lambda}_{\beta,g}^+ - \sum_{\ell:\lambda_\ell>0} \lambda_\ell \{g^{-1}(\alpha\beta_\ell)\}^2 = \mathcal{O}_{a.s.}(n^{-\iota}),$$

is

$$\sum_{\ell=1}^{L_n} \log(1/\beta_\ell) |\widehat{\lambda}_\ell - \lambda_\ell| = \mathcal{O}_{a.s.}(n^{-\iota}), \quad \sum_{\ell>L_n} \log(1/\beta_\ell) (\lambda_\ell)_+ = \mathcal{O}(n^{-\iota}). \quad (14)$$

In fact, since $x \mapsto x_+$ is 1-Lipschitz,

$$|\widehat{\Lambda}^+ - \Lambda^+| \leq \sum_{\ell=1}^{L_n} |\widehat{\lambda}_\ell - \lambda_\ell| + \sum_{\ell>L_n} (\lambda_\ell)_+,$$

and similarly,

$$|\widehat{\Lambda}_\beta^+ - \Lambda_\beta^+| \leq \sum_{\ell=1}^{L_n} \log(1/\beta_\ell) |\widehat{\lambda}_\ell - \lambda_\ell| + \sum_{\ell>L_n} \log(1/\beta_\ell) (\lambda_\ell)_+.$$

Besides, by the tail behavior established in the proof of Theorem 5,

$$\begin{aligned} & \left| \sum_{\ell:\lambda_\ell>0} \lambda_\ell \{g^{-1}(\alpha\beta_\ell)\}^2 - \sum_{\ell:\widehat{\lambda}_\ell>0} \widehat{\lambda}_\ell \{g^{-1}(\alpha\beta_\ell)\}^2 \right| \\ & \leq \sum_{\ell>L_n, \lambda_\ell>0} \lambda_\ell \{g^{-1}(\alpha\beta_\ell)\}^2 + \sum_{\ell=1}^{L_n} |\widehat{\lambda}_\ell - \lambda_\ell| \{g^{-1}(\alpha\beta_\ell)\}^2 \\ & \lesssim \sum_{\ell>L_n, \lambda_\ell>0} \lambda_\ell \log(1/\beta_\ell) + \sum_{\ell=1}^{L_n} |\widehat{\lambda}_\ell - \lambda_\ell| \log(1/\beta_\ell). \end{aligned}$$

For example, if $\beta_\ell \asymp \ell^{-b}$ with $b > 1$ and $L_n \asymp n^a$, the leading term is controlled by

$$\sum_{\ell=1}^{L_n} \log(1/\beta_\ell) |\widehat{\lambda}_\ell - \lambda_\ell| = \mathcal{O}_{a.s.}(n^a (\log n)^{3/2} n^{-1/2}),$$

under the displayed operator-norm rate. Hence, $0 < a < 1/2$ ensures the condition in (14) holds for some small $0 < \iota < 1/2 - a$.